Journal of Power Sources 195 (2010) 7120–7125

Contents lists available at ScienceDirect

Journal of Power Sources

journal homepage: www.elsevier.com/locate/jpowsour

Symmetric redox supercapacitor based on micro-fabrication with three-dimensional polypyrrole electrodes

Wei Sun [a,b], Ruilin Zheng [a,b], Xuyuan Chen [a,b,*]

[a] Institute for Microsystems Technology, Vestfold University College, Tonsberg 3103, Norway
[b] School of Physics and Mechanical & Electrical Engineering, Xiamen University, Xiamen 361005, China

ARTICLE INFO

Article history:
Received 10 February 2010
Received in revised form 4 May 2010
Accepted 9 May 2010
Available online 2 June 2010

Keywords:
Supercapacitor
Microelectromechanical system
Polypyrrole
Specific capacitance
Specific power

ABSTRACT

To achieve higher energy density and power density, we have designed and fabricated a symmetric redox supercapacitor based on microelectromechanical system (MEMS) technologies. The supercapacitor consists of a three-dimensional (3D) microstructure on silicon substrate micromachined by high-aspect-ratio deep reactive ion etching (DRIE) method, two sputtered Ti current collectors and two electrochemical polymerized polypyrrole (PPy) films as electrodes. Electrochemical tests, including cyclic voltammetry (CV), electrochemical impedance spectroscopy (EIS) and galvanostatical charge/discharge methods have been carried out on the single PPy electrodes and the symmetric supercapacitor in different electrolytes. The specific capacitance (capacitance per unit footprint area) and specific power (power per unit footprint area) of the PPy electrodes and symmetric supercapacitor can be calculated from the electrochemical test data. It is found that NaCl solution is a good electrolyte for the polymerized PPy electrodes. In NaCl electrolyte, single PPy electrodes exhibit 0.128 F cm^{-2} specific capacitance and 1.28 mW cm^{-2} specific power at 20 mV s^{-1} scan rate. The symmetric supercapacitor presents 0.056 F cm^{-2} specific capacitance and 0.56 mW cm^{-2} specific power at 20 mV s^{-1} scan rate.

1. Introduction

In the field of energy storage, two main parameters are fundamental for storage devices: the energy density and the power density. The first parameter defines the amount of energy that can be stored in a given volume or weight, while the second parameter describes the speed this stored energy can be stored into or discharged from the device. The ideal storage device should simultaneously have both high energy density, and high power density. Supercapacitors provide higher power density than batteries and higher energy density than conventional capacitors, with moderate high energy density and power density. In addition, supercapacitors have excellent reversibility and long cycle life [1,2]. On the basis of electrode materials used and the charge storage mechanisms, supercapacitors can be classified into: (a) electric double layer capacitors which employ carbon or other materials with large surface area as electrodes [3,4], and (b) redox supercapacitors in which electroactive materials such as transition metal oxides [5] or conducting polymers [6] are applied as electrodes. Generally, the redox supercapacitor has been proved to have a higher capacitance than the electric double layer capacitor. Polypyrrole (PPy) is one of the most promising materials for the electrodes of redox supercapacitor due to its fast charge/discharge kinetics, low cost, facile synthesis and high energy density [7,8]. The electrochemical properties of PPy based electrodes depend on the electrodes preparation methods and also the effective surface area of the electrodes. So far, research groups worldwide have mainly focused on modification of PPy based materials, such as optimizing the conditions of PPy preparation including current density, pH value, temperature, concentration of pyrrole (Py) monomer, types and concentrations of doping ions [9], and preparing PPy based composite films to achieve larger effective surface area by nanotechnology [10–12]. But there is much less attention on increasing the specific capacitance of supercapacitor (or electrode of supercapacitor) by structuring the substrate of the supercapacitor with large effective surface area for PPy electrodes deposition. In this work, we try to shape a substrate with large effective surface area for supercapacitor by employing MEMS technologies.

To the best of our knowledge, there are some methods to fabricate 3D structures by MEMS technologies, including both bulk micromachining and surface micromachining. One way is sing LIGA-like (LIGA is a German acronym for Lithographie, Galvanoformung, Abformung, which mean Lithography, Electroplating and Molding) technology based on thick resist photolithography and electroforming [13], another approach is based on carbon-MEMS [14], and DRIE is also applied for the purpose. DRIE is high-aspect-

* Corresponding author at: Institute for Microsystems Technology, Vestfold University College, Raveien 197, Horten, 3103 Vestfold, Norway. Tel.: +47 33031161; fax: +47 33031103.
E-mail address: xuyuan.chen@hive.no (X. Y. Chen).

0378-7753/$ – see front matter © 2010 Elsevier B.V. All rights reserved.
doi:10.1016/j.jpowsour.2010.05.012

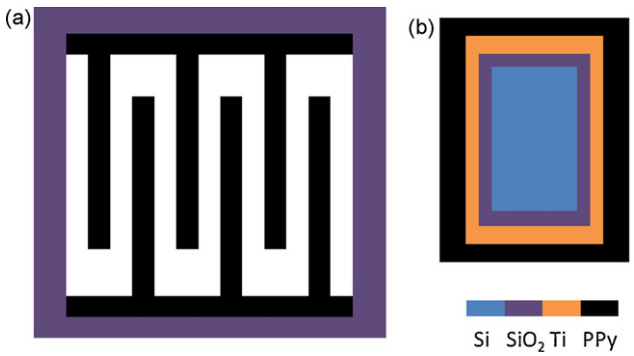

Fig. 1. (a) Schematic drawing of designed supercapacitor and (b) cross-section.

ratio process for fabricating 3D structure on different materials with good quality [15]. Nathan's group fabricated 3D thin film micro-battery by DRIE, which had several times in surface area and specific capacity gain for a given footprint [16]. Jiang fabricated a double layer supercapacitor utilizing vertically aligned carbon nanotube forests with 80 μm height on silicon wafer, and obtained a capacitance density of 428 $\mu F\,cm^{-2}$ and power density of 0.28 $mW\,cm^{-2}$ [17]. MEMS supercapacitors have much larger power density than microbatteries, so it can be used to store energy temporarily and provide pulse power, or in other potential applications where high power is required.

In this study, to achieve both higher energy density and power density, we designed and fabricated a 3D symmetric supercapacitor by MEMS technologies. The key steps in our developed process flow include DRIE for "through-structure" etching, thermal oxidation for SiO_2 growing, RF (radio frequency) sputtering for Ti current collectors depositing and electrochemical polymerization for PPy synthesis. Then the electrochemical behaviors of the PPy electrodes and the symmetric MEMS supercapacitor were investigated by electrochemical tests.

2. Design and experimental

A supercapacitor must include a substrate, current collectors, anode, cathode and electrolyte. If the same materials are used as the anode and the cathode for the supercapacitor, it is called symmetric supercapacitor; otherwise it will be called asymmetric supercapacitor. We designed a 3D redox symmetric supercapacitor as shown in Fig. 1. The supercapacitor has a 3D "through-structure", which includes two disconnected periodic beams surrounded by PPy films serve as anode and cathode of the supercapcitor. For the silicon substrate with thickness of 525 μm and area of 1 cm^2, the interdigitated beams (width of 100 μm) provide more than 10 times effective surface area than similarly planar structure does for a same footprint.

We successfully developed the process flow for fabricating the supercapacitor, which is shown in Fig. 2.

2.1. Structuring silicon substrate

Because etching through the whole 525 μm thickness of the silicon substrate is a time consuming job, patterned Cr layer was used instead of SiO_2 as the DRIE protection mask. Al layer on the back side of the Si wafer serves as DRIE stop layer. Fig. 3(a) presents the photo of the substrate after Cr protection layer patterning. Then the key step DRIE was carried out on AMS200 (Alcatel, France) by using alternating SF_6 and C_4F_8 as etching gas and passivation gas, respectively. We achieved an about 7 $\mu m\,min^{-1}$ etching speed in the first 30 min, then "black silicon" [18] with the grass-like structure occurred on the bottom of the being etched channel. Fig. 3(b) shows the morphology of the "black silicon", we can see that the length of the "grasses" is at the level of hundreds of micrometers. The "black silicon" is caused by etching on different opening area simultaneously. In area with big width, the heat produced cannot be dissipated immediately, then temperature difference occurred on the substrate. In the area with small width, the organic passivation residue cannot be removed completely for next etching cycle. The "black silicon" was eliminated by changing the composite of etching gas, but the etching speed became slower significantly, the total DRIE time is 210 min. It is well known that the lag effect always happens when the width difference of etching area exists [19]. In our experiment, when the area with big width is etched through the whole substrate, there is still 68 μm thick silicon remaining at the region with small width. So the lag effect is about 12.95% (as shown in Fig. 3(c)). To etch away the remaining silicon, an isotropic wet etching solution HF/HNO_3/HAc (acetic acid) was conducted after removing the metal layers of Cr and Al. The HF/HNO_3/HAc solution can also reduce the stress at edges and coarsen the surface for all effective surfaces, as shown in Fig. 3(d). Fig. 3(e) gives the final 3D photo of microfabricated 3D structure taken by Olympus OLS1200 laser scanning confocal microscope.

2.2. Current collectors

After DRIE, a layer of thermal oxidized SiO_2 with thickness of 1.5 μm formed on all the effective surfaces of the 3D structure as insulator. Then continuous Ti layer was deposited on all the tops, bottoms and side walls of the substrate by two-step sputtering (front and back sides). The substrate was rotated at 20 rotations per minute during the sputtering process. Finally, the Ti layer was divided into anodic and cathodic current collectors by etching away the supporting frame.

2.3. Electroactive electrodes

Electroactive PPy films were electrochemical polymerized on current collectors as the electrodes of supercapacitor. The electrochemical polymerizations for single electrodes were carried out at 20 °C under constant 0.8 V voltage for 5–20 min in a electrolytic bath with stirring, which containing 0.5 M Py monomer and 0.3 M sodium p-toluenesulfonate (TOSNa) as surfactant and supporting salt. Additional p-toluenesulfonate acid (TOSH) was applied to adjust the pH of the solution as 4.00. Py (Fluka, 99%) was purified

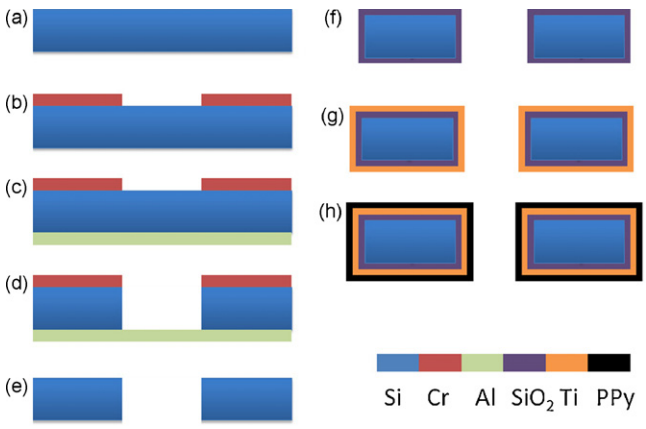

Fig. 2. Process flow for fabricating 3D MEMS supercapacitor. (a) Silicon wafer, (b) Cr mask deposition and patterning, (c) Al back-side deposition, (d) DRIE through the whole thickness of Si wafer, (e) metal layers removal, (f) thermal oxidation, (g) Ti current collectors sputtering, and (h) PPy electrodes eletropolymerization.

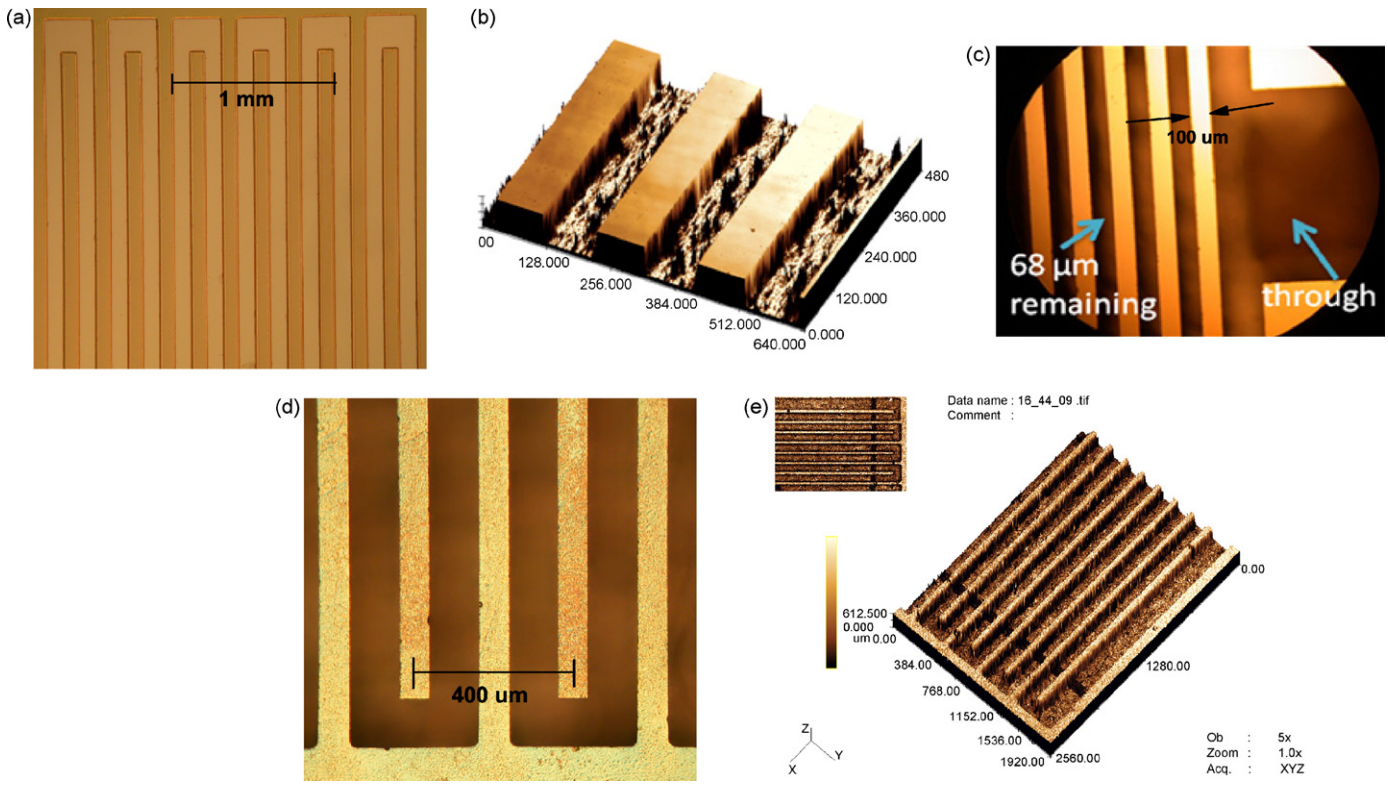

Fig. 3. Detailed DRIE process. (a) After Cr mask patterning, (b) morphology of "black silicon", (c) lag effect of DRIE, (d) after coarsening, and (e) image of microfabricated 3D "through-structure" by Olympus OLS1200 laser scanning confocal microscope.

by vacuum distillation prior to use. Analytical reagent TOSNa and TOSH were obtained from commercial sources and used as received.

2.4. Electrolytes and test methods

TOSNa and NaCl electrolytes with pH 4.00 were used for investigating the electrochemical performance of our 3D symmetric redox MEMS supercapacitor. Cyclic voltammetry (CV), electrochemical impedance spectroscopy (EIS) and galvanostatical charge/discharge were carried out on electrochemical workstation (Solartron 1260) with both two-electrode system and three-electrode system. In three-electrode system, each PPy electrode was used as working electrode, with a platinum sheet as counter electrode, and saturated calomel electrode (SCE) as reference electrode. All the potentials which will be mentioned later in three-electrode system are versus SEC. In two-electrode system, the two PPy electrodes served as the working electrode and the counter electrode, respectively.

3. Results and discussions

For each PPy electrode and the supercapacitor, CV tests were carried out with scan rates ranged from 10 to 100 mV s^{-1}. The specific charge capacitance (C_{charge}) and discharge capacitance ($C_{discharge}$) can be calculated by integrating the current of the CV curve in the half charge cycle and half discharge cycle, respectively. EIS tests were performed from 100 kHz frequency to 10 mHz frequency with the potential amplitude of 10 mV, the specific capacitance can be obtained by simulating the EIS data with a suitable equivalent circuit on the software which is attached to electrochemical workstation. Galvanostatical charge/discharge curves were obtained at the current density from 0.5 to 5 mA cm^{-2}, and the discharge capacitance $C_{discharge}$ was calculated from the linear part of discharge curve by Eq. (1):

$$C_{discharge} = \frac{I \times \Delta t}{\Delta V \times A} \quad (1)$$

where I is the current density applied on PPy electrode or the supercapacitor, Δt is the discharge time from the highest potential to the lowest potential, ΔV is the potential window and A is the surface area of the substrate.

The specific power P of the PPy electrode or the supercapacitor can be calculated from CV and galvanostatical discharge curves by Eq. (2), in which E is the specific energy of the PPy electrode or the supercapacitor.

$$P = \frac{E}{\Delta t} = \frac{C_{discharge} \times \Delta V^2}{2\Delta t} = \frac{I \times \Delta V}{2A} \quad (2)$$

3.1. Effect of electrolytes

0.5 M NaCl solution and TOSNa solution both adjusted to pH 4.00 were used as test electrolytes for single PPy electrode (10 min polymerization) in three-electrode system. The electrochemical behaviors of PPy electrode are shown in Fig. 4.

CV tests of the single PPy electrode were carried out with potential ranged from −0.6 to 0.4 V at scan rate of 20 mV s^{-1}, which are given in Fig. 4(a). In TOSNa electrolyte, the CV curve presents non-ideal capacitance character. While charging, the reactive current increases slowly with the value less than 0.0005 A at potential from −0.6 to 0.2 V, corresponding the oxidation reaction at the interface between PPy electrode and TOSNa electrolyte. However, it increases dramatically when the potential is up to 0.2 V, which means the TOS^- can break the "steric hindrance" caused by shrinking of PPy during discharging [20], and penetrate into the deep position of PPy matrix at charging potential up to 0.2 V. In NaCl electrolyte, the PPy electrode performed ideal capacitance property with rectangle-like shape and higher reactive current about

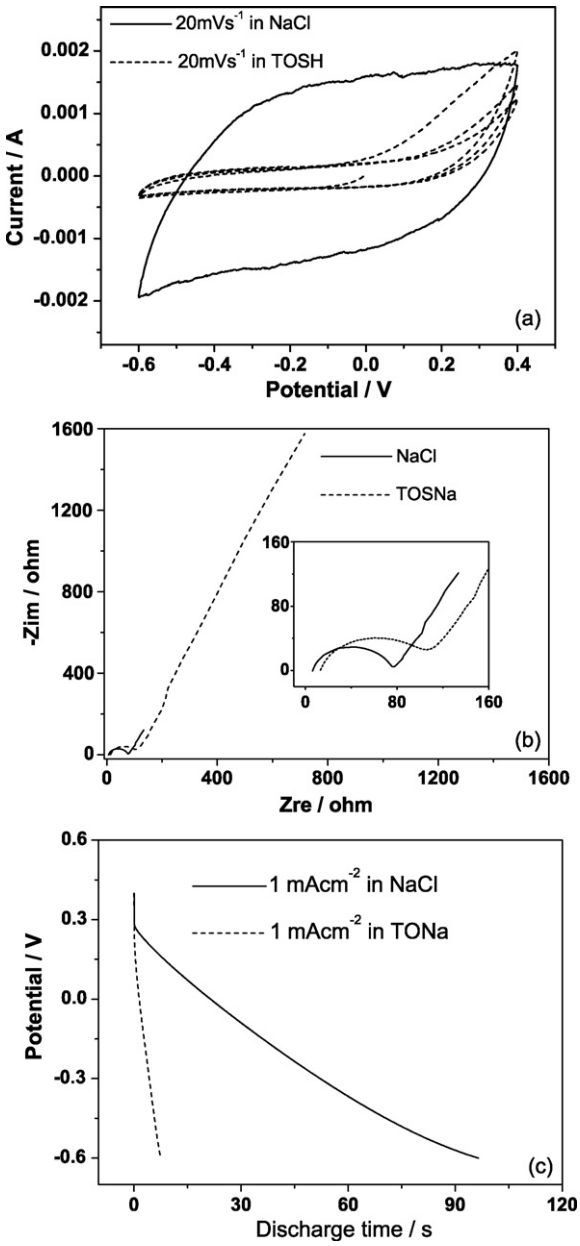

Fig. 4. Electrochemical behaviors of single PPy electrode in NaCl electrolyte and TOSNa electrolyte. (a) CV tests at scan rate of 20 mV s^{-1}, (b) EIS tests at open circuit potential, and (c) galvanostatical charge/discharge tests at discharge rate of 1 mA cm^{-2}.

0.0015 A. This is because Cl^- has smaller size so that can penetrate into very deep position of the PPy film through the "path" formed by TOS^- undoping at the whole test potential range.

EIS curves of the single PPy electrodes were obtained at open circuit potential, as shown in Fig. 4(b). The EIS data can be fitted by the equivalent circuit shown in Fig. 5, in which R_1 represents the resistance of solution and wires, R_2 characterizes the ions transfer resistance from the interface between the electrolyte and the PPy electrode to the deep position of the PPy electrode, and two constant phase elements CPE_1 and CPE_2 instead of pure capacitors were used to describe the double layer capacitance at the interface between the electrolyte and the PPy electrode, and the pseudo capacitance of ions transfer in the PPy matrix, respectively. In high frequency area, depressed semi-circles are observed which implies the electrostatic absorption mechanisms at the interfaces between electrolytes and PPy electrodes (electric double layer capacitance). Because of the roughness of electrodes, there is some dispersion of the double layer capacitance and thus the depressed semi-circles can be better fitted by using CPE_1. While in low frequency area, inclined lines were observed on impedances, the angles between the inclined lines and the real axes are between 45° and 90°, corresponding the ion diffusion mechanism between Warburg diffusion and ideal capacitive ion diffusion (pseudo capacitance). CPE_2 was used for presenting the ions transfer processes to get better fitting results because the thickness of the PPy electrodes is not homogenous in micro-scale. The minus imaginary part ($-Z_{im}$) of the EIS curve for PPy electrode in NaCl electrolyte is much smaller than that in TOSNa electrolyte, and it is well known that the value of pseudo capacitance is in direct proportion to $(-Z_{im})^{-1}$ [21], so the PPy electrode exhibited higher pseudo specific capacitance NaCl electrolyte compare to that in TOSNa electrolyte.

Fig. 5. Equivalent circuit for simulating EIS data.

The galvanostatical discharge tests for the single PPy electrode are shown in Fig. 4(c), with the potential range from −0.6 to 0.4 V at the current density of 1 mA cm^{-2}. It is observed that the discharge time in NaCl electrolyte is much larger than that in TOSNa electrolyte, which means the single PPy electrode can store much more energy with NaCl electrolyte than TOSNa electrolyte.

The specific capacitance and specific power calculated from CV, EIS and galvanostatical discharge tests are given in Table 1. Obviously, PPy electrode in NaCl electrolyte bears much larger specific capacitance than that in TOSNa electrolyte for the all three test methods. The capacitance of PPy actually comes from the reversible p-type doping and undoping of anions. The PPy electrode as prepared is doped with TOS^- and different reactions happened in NaCl electrolyte and TOSNa electrolyte are described by the following formulas.

$$PPy^+TOS^- + e \rightarrow PPy + TOS^- \quad (3)$$

$$PPy + TOS^- - e \rightarrow PPy^+TOS^- \quad (4)$$

$$PPy + Cl^- - e \rightarrow PPy^+Cl^- \quad (5)$$

$$PPy^+Cl^- + e \rightarrow PPy + Cl^- \quad (6)$$

In TOSNa electrolyte, reactions described by Eqs. (3) and (4) occurred during discharging and charging. In NaCl electrolyte, reaction depicted by Eq. (3) occurred at the first discharge half cycle, but the Cl^- replace of the TOS^- in the next charge and discharge due to its larger concentration and smaller size, as shown in Eqs. (5) and (6). Due to the smaller size and higher ionic mobility of Cl^- in comparison to TOS^-, Cl^- can go into very deep position of the PPy film easily through the "path" formed by TOS^- undoping, thus the PPy electrode presents batter capacitance behaviors in NaCl electrolyte, with the specific capacitance values much larger than that in TOSNa electrolyte, as shown in Table 1.

We also found that the PPy electrode in NaCl electrolyte also exhibited much larger specific power than that in TOSNa electrolyte at the same CV scan rate, which means in a same discharge time, PPy electrode can provide much higher power density. While in the galvanostatical discharge tests with the same discharge current density, the specific powers of PPy electrodes are the same in both electrolytes, but the discharge time of PPy electrode is much shorter in TOSNa electrolyte than that in NaCl electrolyte.

Table 1
Specific capacitance and power from CV (20 mV s^{-1}), EIS and galvanostatical discharge (1 mA cm^{-2}).

	Electrolyte					
	NaCl			TOSNa		
	Test method					
	CV	EIS	Galvanostatical discharge	CV	EIS	Galvanostatical discharge
Specific capacitance (F cm^{-2})	0.079	0.060	0.096	0.011	0.006	0.008
Specific power (mW cm^{-2})	0.79		0.50	0.11		0.50

In a word, NaCl electrolyte is more suitable than TOSNa electrolyte for our PPy electrode of supercapacitor.

3.2. Effect of polymerization time

Single PPy electrodes polymerized for 5, 10 and 20 min were electrochemical investigated by CV and galvanostatical discharge methods with three-electrode system in NaCl electrolyte. Fig. 6(a) and (b) illustrates the CV and galvanostatical discharge curves of PPy electrodes at scan rate of 20 mV s^{-1} and current density of 1 mA cm^{-2}, respectively. With the increasing polymerization time, the reactive currents of CV curves and the discharge time of galvanostatical discharge curves rise almost proportionally, which correspond the linear relationship between the calculated specific capacitance and polymerization time, as shown in Fig. 6(c).

The PPy electrodes polymerized for 5, 10 and 20 min were also tested with various scan rates from 5 to 100 mV s^{-1}. The specific capacitances at different scan rates are shown in Fig. 7(a). Besides the linear relationship between specific capacitance and polymerization time, it is found that the specific capacitance decreased rapidly as scan rate increasing from 5 to 20 mV s^{-1}, but slowly with scan rate increasing from 20 to 100 mV s^{-1} for each PPy electrode. This is because that at fast scan rate, the charge diffusion cannot follow the change of electric field, which gives rise to smaller specific capacitance, while at slow scan rate, ion doping/undoping is finished completely over long time, resulting in large capacitance. The specific powers at different scan rates are shown in Fig. 7(b). It is obviously that the specific power increase with both increasing polymerization time and scan rate. When the PPy electrode polymerized for 20 min charge and discharge with CV scan rate of 100 mV s^{-1}, the highest specific power value 4.05 mW cm^{-2} is achieved, corresponding to a specific capacitance of 0.081 F cm^{-2}.

3.3. Performance of supercapacitor in one chip

The symmetric supercapacitor consisted of two PPy electrodes polymerized for 20 min was test with two-electrode system in NaCl electrolyte. One PPy electrode served as working electrode and the other electrode is counter electrode. Fig. 8 presents the CV curve of the supercapacitor with the potential range from −1.0 to 1.0 V at the scan rate of 20 mV s^{-1}. The rectangle shape of the curve shows obviously ideal supercapacitor performance. In practice, the symmetric supercapacitor can be charged on both PPy electrodes without any difference. By the crossed lines of zero potential and zero current, the CV curve was divided into two charging parts and two discharging parts which are shown in Fig. 8. The charge or discharge capacitances can be calculated by integrating the current of the CV curve in one fourth of the cycle. The average specific charge and discharge capacitances of the symmetric supercapacitor are 0.085 and 0.056 F cm^{-2}. Theoretically, the capacitance of the symmetric supercapacitor should be equal to the capacitance of the two PPy electrodes connected in series, i.e. half of the capacitance of single PPy electrode. Here, the value of 0.056 F cm^{-2} is lightly smaller than that half of the specific capacitance of one PPy electrode 0.064 F cm^{-2} (0.5 × 0.128, in Fig. 7(a)). The specific discharge power of the supercapacitor is calculated as 0.56 mW cm^{-2}.

Galvanostatical charge/discharge curve of the symmetric supercapacitor at current density of 5 mA cm^{-2} with the potential ranged from −1.0 to 1.0 V is shown in Fig. 9. Both charge and discharge lines

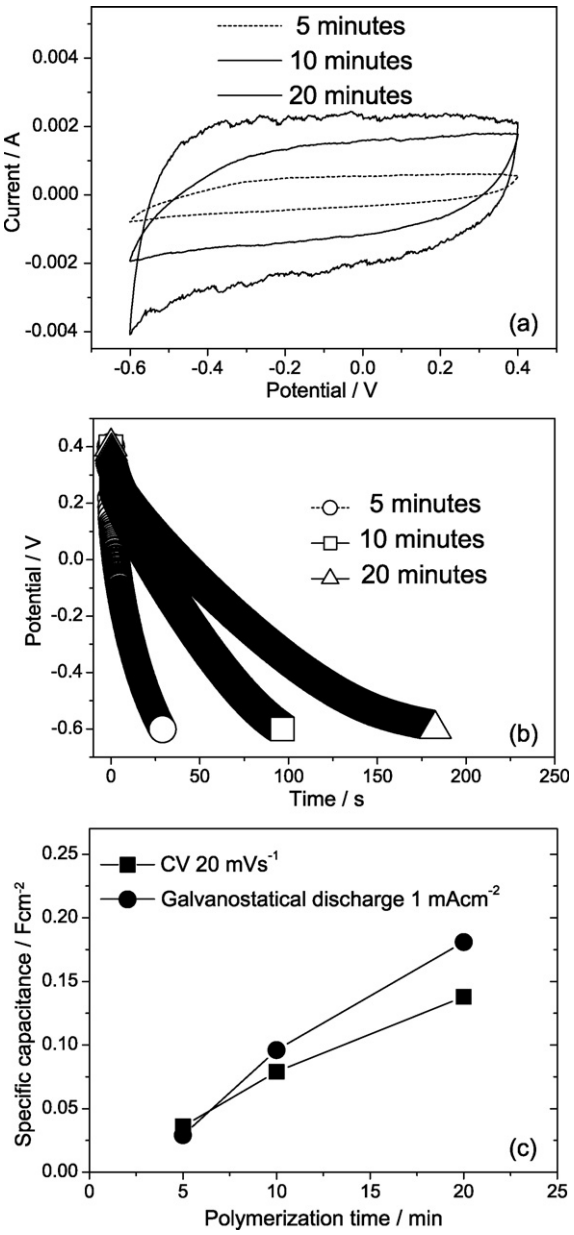

Fig. 6. Electrochemical behavior of single PPy electrodes with various polymerization times. (a) CV at scan rate of 20 mV s^{-1}, (b) galvanostatical discharge curve at current density of 1 mA cm^{-2}, and (c) specific capacitances versus polymerization time.

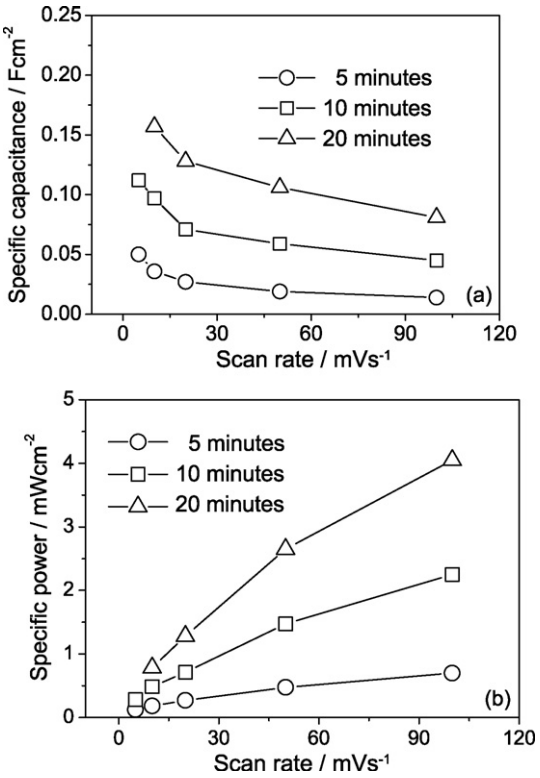

Fig. 7. (a) Specific capacitances and (b) specific powers of single PPy electrodes polymerized for 5, 10 and 20 min at various scan rates from 5 to 100 mV s^{-1}.

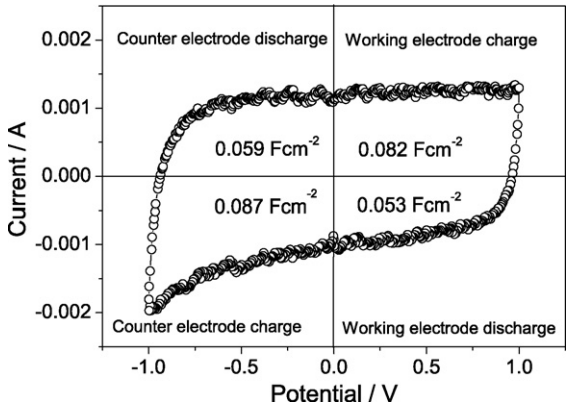

Fig. 8. CV of the symmetric supercapacitor with two PPy electrodes polymerized for 20 min.

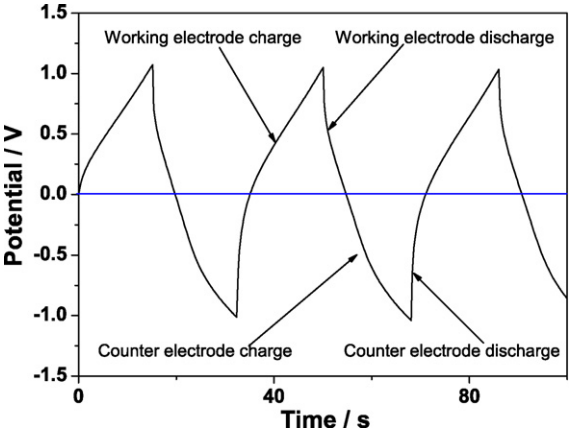

Fig. 9. Galvanostatical charge/discharge curve of the symmetric supercapacitor.

are almost linear, which means good capacitance property of the symmetric supercapacitor. One charge/discharge cycle can also be divided into four parts, corresponding the charging and discharging of working electrode and counter electrode, respectively, as shown in Fig. 9.

4. Conclusions

A symmetric redox 3D supercapacitor was designed and fabricated by MEMS technologies. The supercapacitor consists of a silicon substrate, Ti current collectors and PPy electrodes. DRIE was used to etch through the whole thickness of the silicon substrate to form the interdigitated 3D structure, which significantly enlarge the effective surface area of the substrate. Continuous Ti layers and PPy films were deposited on the 3D structure as current collectors and electrodes, respectively. CV, EIS and galvanostatical charge/discharge methods were used to investigate the behaviors of single PPy electrodes and the symmetric supercapacitor. It is found that NaCl solution was the suitable electrolyte for our PPy electrodes for supercapacitor. In NaCl electrolyte, the single PPy electrodes can present 0.128 F cm^{-2} specific capacitance and 1.28 mW cm^{-2} specific power at 20 mV s^{-1} scan rate. The symmetric supercapacitor with two identical PPy electrodes polymerized for 20 min has 0.056 F cm^{-2} specific capacitance and 0.56 mW cm^{-2} specific power at 20 mV s^{-1} scan rate. The symmetric 3D MEMS supercapacitor is promising in MEMS application, especially in where high power is required.

Acknowledgements

The authors thank the MEMS fabrication helping by Pen-Tung Sah MEMS research center in Xiamen University and the electrochemical tests helping by State Key Laboratory for physical chemistry of solid surfaces in Xiamen University.

References

[1] K.S. Ryu, K.M. Kim, N.G. Park, Y.J. Park, S.H. Chang, Journal of Power Sources 103 (2002) 305–309.
[2] Y. Xue, Y. Chen, M.L. Zhang, Y.D. Yan, Materials Letters 62 (2008) 3884–3886.
[3] A. Tanimura, A. Kovalenko, F. Hirata, Chemical Physics Letters 378 (2003) 638–646.
[4] D.A. Brevnov, T.S. Olson, Electrochimica Acta 51 (2006) 1172–1177.
[5] Z.A. Hu, Y.L. Xie, Y.X. Wang, L.P. Mo, Y.Y. Yang, Z.Y. Zhang, Materials Chemistry and Physics 114 (2009) 990–995.
[6] S.R. Sivakkumar, W.J. Kim, J.A. Choi, D.R. MacFarlane, M. Forsyth, D.W. Kim, Journal of Power Sources 171 (2007) 1062–1068.
[7] J.H. Kim, A.K. Sharma, Y.S. Lee, Materials Letters 60 (2006) 1697–1701.
[8] B.L. He, Y.K. Zhou, W.J. Zhou, B. Dong, H.L. Li, Materials Science and Engineering A 374 (2004) 322–326.
[9] R.K. Sharma, A.C. Rastogi, S.B. Desu, Electrochemistry Communications 10 (2008) 268–272.
[10] A. Laforgue, P. Simon, C. Sarrazin, J.F. Fauvarque, Journal of Power Sources 80 (1999) 142–148.
[11] C. Weidlich, K.M. Mangold, K. Juttner, Electrochimica Acta 50 (2005) 1547–1552.
[12] Y.L. Xu, J. Wang, W. Sun, S.H. Wang, Journal of Power Sources 159 (2006) 370–373.
[13] C. Maleka, V. Saileb, Microelectronics Journal 35 (2004) 131–143.
[14] H.S. Min, B.Y. Park, L. Taherabadi, C. Wang, Journal of Power Sources 178 (2008) 795–800.
[15] C.M. Waits, B. Morgan, M. Kastantin, R. Ghodssi, Sensors and Actuators A 119 (2005) 245–253.
[16] M. Nathan, D. Golodnitsky, V. Yufit, E. Strauss, T. Ripenbein, I. Shechtman, S. Menkin, E. Peled, Journal of Microelectromechanical Systems 14 (2005) 879–885.
[17] Y.Q. Jiang, Q. Zhou, L. Lin, Micro Electro Mechanical Systems, 2009. MEMS 2009 IEEE 22nd International Conference, Sorrento, Italy, 25–29 January, 2009.
[18] Y. Fintschenko, A. van den Berg, Journal of Chromatography A 819 (1998) 3–12.
[19] Y.Y. Tan, R.C. Zhou, H.X. Zhang, G.Z. Lu, Z.H. Li, Journal of Micromechanics and Microengineering 16 (2006) 2570–2575.
[20] T.F. Otero, J. Padilla, Journal of Electroanalytical Chemistry 561 (2004) 167–171.
[21] J. Wang, Y. Xu, X. Chen, X. Sun, Composites Science and Technology 67 (2007) 2981–2985.